30. Beclin, C., Boutet, S., Waterhouse, P. & Vaucheret, H. A branched pathway for transgene-induced RNA silencing in plants. *Curr. Biol.* **12,** 684–688 (2002).

Supplementary Information accompanies the paper on **www.nature.com/nature**.

Acknowledgements This research was supported by grants from AIST and by a Grant-in-Aid for Scientific Research and for the 21st Century COE programmes, Center for Integrated Brain Medical Science and Human-Friendly Materials based on Chemistry, from the Ministry of Education, Culture, Sports, Science and Culture (MEXT) of Japan.

Competing interests statement The authors declare that they have no competing financial interests.

Correspondence and requests for materials should be addressed to K.T. (taira@chembio.t.u-tokyo.ac.jp) or H.K. (kawasaki@chembio.t.u-tokyo.ac.jp).

Error-prone replication of oxidatively damaged DNA by a high-fidelity DNA polymerase

Gerald W. Hsu[1], Matthias Ober[2], Thomas Carell[2] & Lorena S. Beese[1]

[1]*Department of Biochemistry, Duke University Medical Center, Durham, North Carolina 27710, USA*
[2]*Department of Chemistry and Biochemistry, Ludwig Maximilians University Munich, Butenandtstrasse 5-13, D 81377 Munich, Germany*

Aerobic respiration generates reactive oxygen species that can damage guanine residues and lead to the production of 8-oxoguanine (8oxoG), the major mutagenic oxidative lesion in the genome[1]. Oxidative damage is implicated in ageing[2] and cancer, and its prevalence presents a constant challenge to DNA polymerases that ensure accurate transmission of genomic information. When these polymerases encounter 8oxoG, they frequently catalyse misincorporation of adenine in preference to accurate incorporation of cytosine[3]. This results in the propagation of G to T transversions, which are commonly observed somatic mutations associated with human cancers[4,5]. Here, we present sequential snapshots of a high-fidelity DNA polymerase during both accurate and mutagenic replication of 8oxoG. Comparison of these crystal structures reveals that 8oxoG induces an inversion of the mismatch recognition mechanisms that normally proofread DNA, such that the 8oxoG·adenine mismatch mimics a cognate base pair whereas the 8oxoG·cytosine base pair behaves as a mismatch. These studies reveal a fundamental mechanism of error-prone replication and show how 8oxoG, and DNA lesions in general, can form mismatches that evade polymerase error-detection mechanisms, potentially leading to the stable incorporation of lethal mutations.

Many DNA damage lesions stall or block DNA replication; however, 8oxoG is bypassed efficiently and inaccurately by high-fidelity polymerases[3,6–8]. 8oxoG retains the ability to engage in correct Watson–Crick base pairs with C, but oxidation of G (at C8) converts a hydrogen bond acceptor (N7) to a hydrogen bond donor, allowing a stable Hoogsteen base pair to form between 8oxoG and A, which is not possible in undamaged DNA (Fig. 1). In the absence of accessory factors such as proliferating cell nuclear antigen (PCNA), preferential mutagenic translesion replication of 8oxoG by the major replicative DNA polymerases α and δ *in vitro* indicates that 8oxoG is not recognized as a DNA lesion. Instead, the A·8oxoG mismatch evades the intrinsic mechanisms that cause DNA polymerases to achieve high-fidelity replication of undamaged DNA.

Insights into the mechanisms of faithful replication by high-fidelity polymerases[9] and mismatch recognition[10] have been provided by capturing structures of the replication cycle of the DNA polymerase I fragment from a thermostable strain of *Bacillus stearothermophilus* (BF) in a polymerase crystal that retains the ability to replicate DNA[11]. Throughout the replicative cycle of BF, there are many points at which recognition of DNA mismatches or lesions can occur. First, during the transition of the template strand from a pre-insertion site that sequesters the template base before nucleotide incorporation to an insertion site where the template base interacts with the incoming nucleotide, the conformations of the template base and the incoming nucleotide are both tightly regulated to ensure that hydrogen bonding interactions are limited to the Watson–Crick faces of the nascent base pair. Second, before covalent incorporation of the paired dNTP at the insertion site, the polymerase selects for base pairs that exhibit the shape and geometry of cognate Watson–Crick base pairs in preference to ones that do not[12,13]. Third, after covalent incorporation, the new base pair moves to a post-insertion site where residues Arg 615 and Gln 797 form hydrogen bonds to the DNA minor groove of correctly formed base pairs. At this step, DNA mismatches induce distortions within the polymerase active site that cause the polymerase to stall and dissociate[10]. Last, covalently incorporated mismatches or lesions continue to impede replication from up to four base pairs away[14], inducing distortions to the active site as they translocate along the surface of the polymerase[10]. In this way, a molecular 'memory' of the mismatch is retained by the polymerase.

To investigate whether BF behaves analogously to replicative polymerases α and δ with respect to replication of 8oxoG, primer extension assays were performed (Fig. 2) and steady-state kinetic parameters were determined for incorporation of dCTP or dATP opposite 8oxoG (Table 1). Comparison of the specificity constants (k_{cat}/K_m; where k_{cat} is the turnover number and K_m is the Michaelis constant) for incorporation of these nucleotides opposite 8oxoG indicates that misincorporation of dATP is ninefold more efficient than dCTP incorporation, whereas in undamaged DNA, accurate dCTP incorporation opposite an unmodified guanine is 10^6-fold more efficient than misincorporation of dATP. After incorporation of either dATP or dCTP, extension past the newly formed 8oxoG base pair is readily observed (Fig. 2a, b) and proceeds to the end of the template in the presence of a full complement of dNTPs (Supplementary Fig. 1). These results indicate that BF, as with replicative polymerases α and δ, preferentially misincorporates dATP opposite 8oxoG. BF can therefore serve as a model system to address mutagenic 8oxoG replication.

To determine the effects of 8oxoG on the structural mechanisms

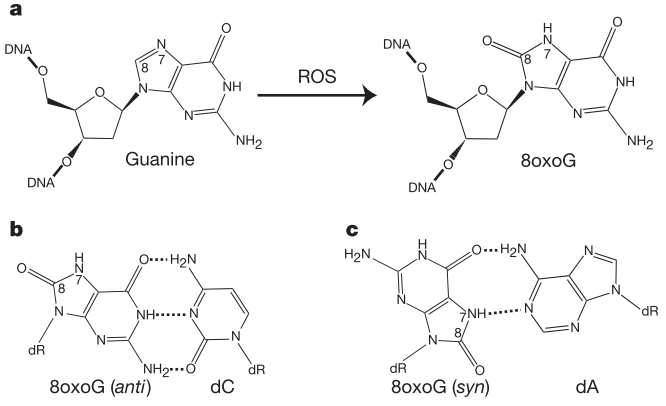

Figure 1 Modes of base pairing for 8oxoG. **a**, Oxidation of guanine at C8 by reactive oxygen species (ROS). **b**, 8oxoG in a Watson–Crick base pair with dC. Dashed lines indicate potential hydrogen bonds. **c**, 8oxoG (*syn*) in a Hoogsteen base pair with dA (*anti*).

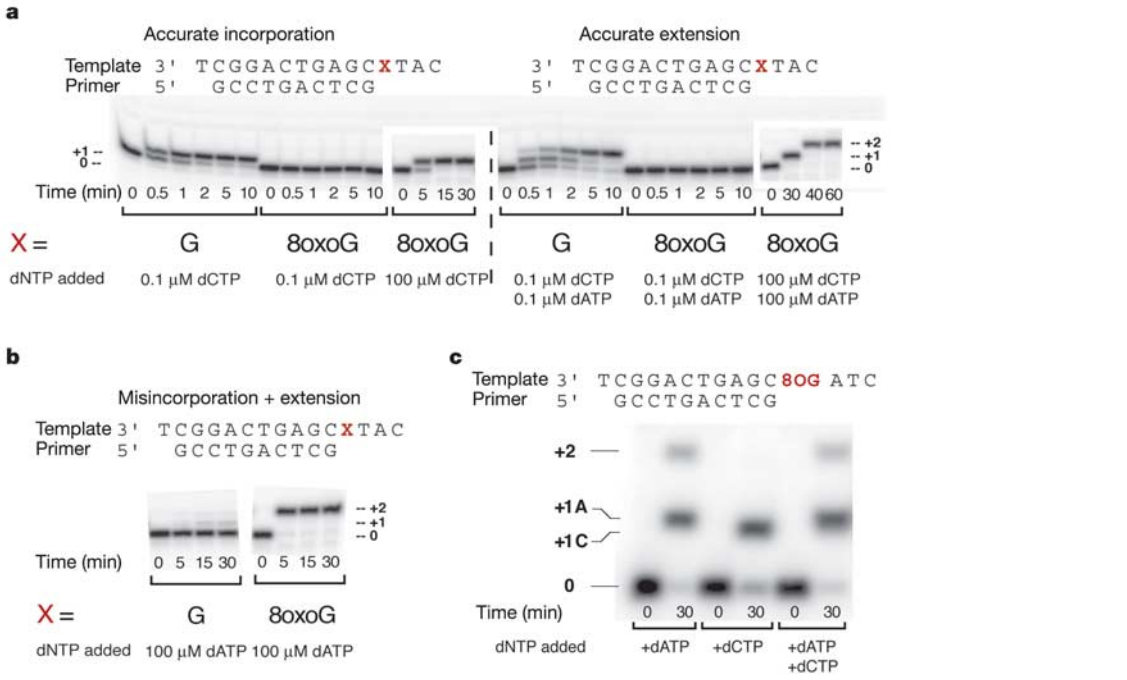

Figure 2 Translesion replication of 8oxoG by BF in solution. **a**, **b**, Accurate (**a**) and mutagenic (**b**) replication of 8oxoG in solution. Primers (10 nucleotides) annealed to templates containing unmodified guanine or 8oxoG at position X were extended by one or two nucleotides. To observe replication of 8oxoG, dNTP concentrations were raised to 100 μM. Extension of C·8oxoG was performed by allowing incorporation of dCTP to occur to completion (30 min) before adding dATP so that extended products exclusively represent extension of C·8oxoG. **c**, In the presence of equimolar amounts of dATP and dCTP (last lane), BF preferentially misincorporates dATP. A quantitative analysis is shown in Table 1.

of mismatch recognition, we obtained sequential structural views of BF as it accurately (Fig. 3; see also Supplementary Fig. 2) and mutagenically (Fig. 4; see also Supplementary Figs 2 and 3) replicated 8oxoG (Table 2). These structures show 8oxoG at the pre-insertion site before nucleotide incorporation, at the post-insertion site after incorporation of dCTP or dATP, and in the DNA duplex binding region after extension of 8oxoG-containing base pairs. The polymerase structure with 8oxoG at the pre-insertion site (Fig. 3b) is similar to that with all other template bases at this position. At the post-insertion site, 8oxoG forms a Watson–Crick base pair with cytosine (Fig. 3c) but a Hoogsteen base pair with adenine (Fig. 4a). At this position, the C·8oxoG (primer·template) base pair disrupts the polymerase active site, but the A·8oxoG base pair does not. However, when either the C·8oxoG or A·8oxoG base pairs occupy the DNA duplex binding region after extension (Figs 3d and 4b), neither distorts the active site.

At the pre-insertion site, 8oxoG resembles a cognate template base and adopts a *syn* conformation (Fig. 3b). Transition of the template base from the pre-insertion site is typically associated with a change to an *anti* conformation at the post-insertion site. This transition remains intact upon incorporation of dCTP but not dATP. By adopting an *anti* conformation to pair opposite cytosine (Fig. 3c), 8oxoG induces template distortion to avoid a potential steric clash between the C8 carbonyl oxygen and the O4′ of the sugar moiety. The relative orientation of the sugar and base is altered, thereby inducing distortion to the template 5′ and 3′ of the lesion. This template distortion is transmitted to the polymerase active site, resulting in active site distortions that resemble those induced by mismatches in undamaged DNA[10]. Template distortions induced by 8oxoG have previously been reported in ternary complex structures of RB69 (ref. 8) and DNA polymerase β[15] bound to an 8oxoG-containing template and an incoming dCTP, indicating that template distortions are initiated before catalysis of the phosphodiester bond and are an intrinsic property of the lesion due to internal steric strain. Here we observe that these distortions affect not only the template but the polymerase as well. The 8oxoG-containing template lifts away from the surface of the polymerase, disrupting the interaction with the minor-groove reading residue Gln 797, and the polymerase O and O1 helices adopt a distorted conformation that prevents the next template base from occupying the pre-insertion site. Similar template and polymerase distortions are observed when DNA mismatches occupy the post-insertion site[10], and account for the inhibitory effect of mismatches on further DNA synthesis[16–18].

Template and polymerase distortions are not observed when 8oxoG adopts a *syn* conformation that enables it to form a Hoogsteen base pair with adenine. In this arrangement, the active site is not disrupted (Fig. 4a). By adopting a *syn* conformation, 8oxoG eliminates internal steric strain, which would cause template distortion. In the Hoogsteen base-pairing arrangement, the surface of the A·8oxoG mismatch resembles a normal Watson–Crick base pair in shape and geometry, and occupies the post-insertion site without distorting the protein, template, or primer. Furthermore, hydrogen bonds between polymerase residues Arg 615 and Gln 797 and the

Table 1 **Steady-state incorporation kinetics**

Template	dNTP	K_m (μM)	k_{cat} (min^{-1})	k_{cat}/K_m ($\mu M^{-1} min^{-1}$)	dCTP:dATP*
8oxoG	dCTP	100.7	13	0.13	
	dATP	46.9	54	1.15	0.11
dG	dCTP	1.5	750	500	
	dATP	111.1	0.007	6.3×10^{-5}	7.9×10^{6}

*Values of k_{cat}/K_m ratio.

A·8oxoG base pair are retained, as the minor groove of A·8oxoG is virtually identical in geometry to the minor groove of a cognate A·T base pair. Therefore, the A·8oxoG mismatch evades mismatch detection. Although Hoogsteen base pairing has been observed to facilitate accurate replication by error prone polymerases[19,20], and has been predicted to allow 8oxoG to form a base pair with A[8,15,21,22], the observation of a template base in a *syn* conformation at the high-fidelity polymerase active site has not been reported previously. Formation of the 8oxoG-induced Hoogsteen base pair is particularly insidious in this context because it promotes the formation of a

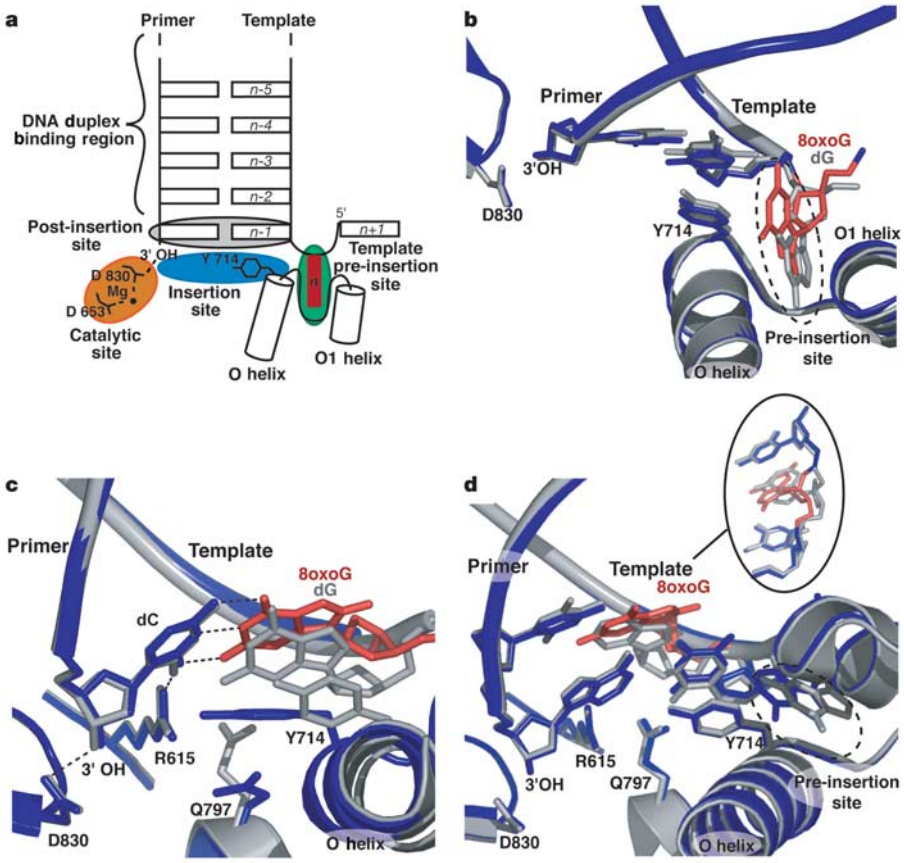

Figure 3 Accurate translesion replication of 8oxoG by BF in crystals. **a**, Schematic of BF active site. During replication, the template base (*n*, red) moves from the pre-insertion site to the post-insertion site to the DNA duplex binding region. **b**–**d**, Structures of accurate 8oxoG replication (blue) are superimposed with structures of unmodified guanine replication (grey). The 8oxoG template base (red) is shown at the pre-insertion site (**b**) before nucleotide incorporation, the post-insertion site (**c**) after dCTP incorporation, and the DNA duplex binding region (**d**) after extension of C·8oxoG.

Table 2 **Summary of crystallographic data**

Crystal	8oxo	C·8oxo	C·8oxo	A·8oxo	A·8oxo
Position of lesion	Pre-IS	Post-IS	*n*-2	Post-IS	*n*-3
Wavelength (Å)	1.542†	1.542†	1.542†	1.542†	1.000‡
Resolution range (Å)	50–2.0	50–2.0	50–2.1	50–2.15	50–1.6
Outer shell (Å)	2.07–2.0	2.07–2.0	2.18–2.1	2.23–2.15	1.66–1.6
R_{sym} (%)*	5.0 (12.2)	9.1 (30.2)	7.5 (24.4)	6.5 (22.4)	7.3 (19.0)
Unique reflections	58,360	59,296	51,291	48,131	114,192
Total reflections	496,318	838,647	668,787	623,476	1,859,662
Mean I/σ_I*	20.3 (6.4)	11.0 (2.6)	10.1 (2.6)	12.3 (3.0)	16.3 (4.4)
Completeness (%)*	92.1 (81.6)	92.9 (86.4)	89.5 (82.9)	90.9 (81.4)	93.8 (75.5)
R_{cryst} (%)	19.4	21.6	20.5	20.5	21.3
R_{free} (%)	22.7	24.7	23.9	24.7	22.7
r.m.s. deviation bond length (Å)	0.005	0.005	0.006	0.006	0.005
r.m.s. deviation bond angle (deg)	1.2	1.2	1.2	1.2	1.2
Average *B*-value (Å^2)	24.1	30.7	29.7	30.6	20.3
Sigma A coordinate error (Å^2)	0.09	0.17	0.21	0.29	0.14

$R_{sym} = (\Sigma|(I - <I>)|)/(\Sigma I)$, where $<I>$ is the average intensity of multiple measurements. R_{cryst} and $R_{free} = (\Sigma||F_o| - |F_c||)/(\Sigma|F_o|)$. R_{free} was calculated over 5% of the amplitudes not used in refinement. r.m.s., root mean square; pre-IS, pre-insertion site; post-IS, post-insertion site. See text for definition.
*Values in parentheses correspond to those in the outer resolution shell.
†Data collected using Rigaku rotating anode X-ray generator.
‡Data collected at beamline 22-ID, APS.

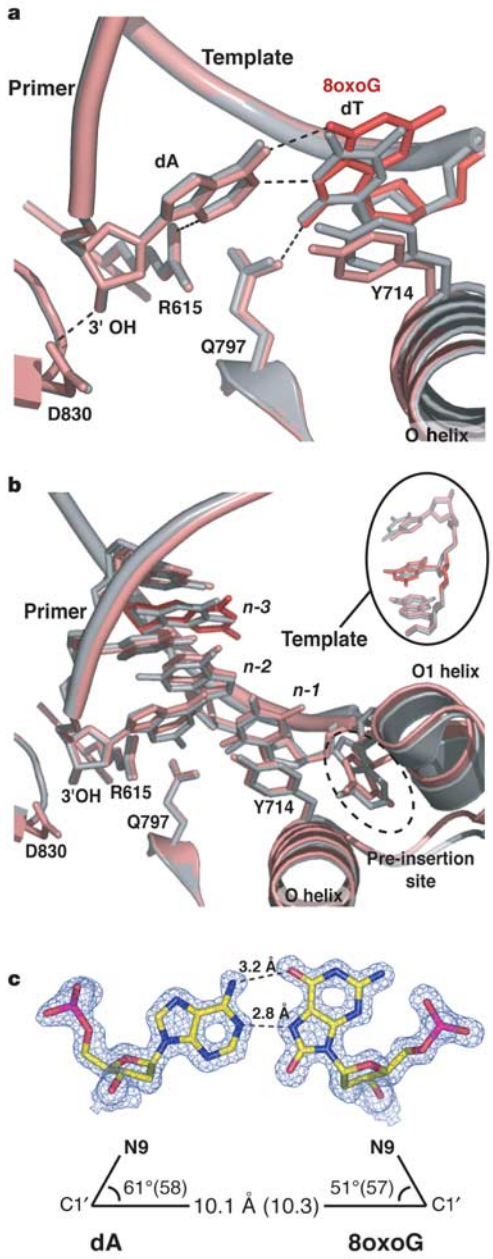

Figure 4 Mutagenic translesion replication of 8oxoG by BF in crystals. **a**, **b**, Structures of mutagenic 8oxoG replication (pink) are superimposed with structures of normal replication (grey). Before dATP incorporation, 8oxoG occupies the pre-insertion site as shown in Fig. 3b. After dATP incorporation, the A·8oxoG mismatch mimics a cognate A·T base pair at the post-insertion site (**a**). No polymerase distortions are observed after extension of the A·8oxoG mismatch (**b**). **c**, Hoogsteen base pairing between dA and 8oxoG with simulated annealing omit electron density (contoured at 4σ). A·8oxoG base pair parameters, with normal parameters for the A·T base pair in parentheses, are shown below.

DNA mismatch that is treated by the polymerase as a normal base pair.

After extension and translocation to the DNA duplex binding region, the A·8oxoG mismatch continues to mimic a cognate base pair, failing to distort the polymerase active site and evading error detection (Fig. 4b). Distortions are also absent after extension of C·8oxoG (Fig. 3d), even though this base pair resembles a DNA mismatch at the post-insertion site. After extension of C·8oxoG, template distortion induced by internal steric strain of the *anti*-8oxoG persists (Fig. 3d, inset), but the distortion is now localized to the site of the base pair and is not transmitted back to the polymerase active site, as are mismatches in undamaged DNA. The absence of long-range distortions is attributable to the stable Watson–Crick or Hoogsteen base-pairing configurations in C·8oxoG and A·8oxoG respectively, whereas base-pairing configurations of mismatches in undamaged heteroduplex DNA are less stable. Distortions induced by mismatch extension represent the final opportunity for the polymerase to recognize a DNA mismatch. By mimicking a cognate base pair, the A·8oxoG mismatch also evades this final error recognition mechanism.

Preferential formation of the A·8oxoG Hoogsteen base pair over the stable C·8oxoG base pair is enabled by guanine oxidation, a process that alters the hydrogen-bonding configurations of the oxidized base. The presence of 8oxoG inverts the molecular logic of mismatch recognition: the correct C·8oxoG base pair is recognized as a mismatch, whereas the mutagenic A·8oxoG base pair mimics the structure of a cognate base pair. Consequently, the incorporation efficiency of C·8oxoG is much less than that of A·8oxoG, accounting for the mutagenic properties of this lesion. This mechanism of error-prone replication of 8oxoG suggests that the mutagenic potential of other types of DNA damage depends in part on their ability to adopt alternative modes of base pairing with mismatched bases that evade polymerase error detection mechanisms. □

Methods

Preparation of protein and DNA

BF was purified as described[23]. DNA oligonucleotides containing 8oxoG (5′-CAT-8oxoG-CGAGTCAGGCT (template 1) and 5′-CTA-8oxoG-CGAGTCAGGCT (template 2)) were synthesized using UltraMILD CE phosphoramidites (trityl off mode). Template oligonucleotides and commercially synthesized complementary primer oligonucleotides were de-protected and purified by reversed-phase high-performance liquid chromatography (HPLC). Template oligonucleotides were analysed by HPLC and matrix-assisted laser desorption ionization–time of flight (MALDI–TOF).

In vitro replication of 8oxoG by BF

The template 15-nucleotide DNA oligonucleotides used for crystallization and an unmodified 15-nucleotide DNA oligonucleotide identical in sequence but with guanine in place of 8oxoG were annealed to a 5′ [^{32}P]-labelled primer (5′-GCCTGACTCG) at a molar ratio of 1:2. For semi-quantitative analyses (Fig. 2), primers were extended (standard 10 μl reactions containing 50 mM Tris pH 8.0, 5 mM $MgCl_2$, 1 mM DTT, 250 μg ml^{-1} BSA, 2.5% glycerol, 10 nM annealed duplex, 1 nM BF, room temperature) with 0.1–100 μM dNTP (dCTP for accurate incorporation opposite 8oxoG; sequential addition of dCTP and dATP for accurate extension past 8oxoG; dATP for misincorporation opposite and accurate extension past 8oxoG). To determine incorporation preference opposite 8oxoG in a competitive reaction, dATP and dCTP were included at equimolar concentrations (100 μM). Control reactions with dATP or dCTP mark the different mobilities of primers extended with dATP or dCTP. Quantitative primer extension reactions to determine nucleotide incorporation kinetics opposite 8oxoG and unmodified guanine used 100 nM duplex DNA with BF concentrations and reaction times optimized to ensure linearity and single hit kinetics (<20% of primers extended under steady-state conditions)[17,24]. Concentrations of the dATP or dCTP varied from 0 to 2 mM. Reactions were performed at 25 °C and terminated by addition of 10 μl 95% formamide/10 mM EDTA and heating to 95 °C for 10 min. Primers and products were separated by electrophoresis (20% polyacrylamide/7 M urea) and quantified (Molecular Dynamics Storm 840 Phosphorimager). Michaelis constant (K_m) and V_{max} values were determined by a least-squares nonlinear fit of the data to the Michaelis–Menten equation (Supplementary Data 1).

Catalysis in the crystal and structure determination

Crystals of BF bound to DNA duplex containing 8oxoG at the pre-insertion site were grown as described[9,11]. Accurate incorporation of 8oxoG was observed in crystals of BF bound to template 1 soaked in a solution (60% saturated ammonium sulphate, 0.1 M Tris pH 8.0, and 2.5% MPD) with 30 mM dCTP. C·8oxoG was extended by soaking BF-DNA duplex crystals containing an enzymatically incorporated C·8oxoG base pair at the post-insertion site in a 30 mM dATP soak solution. Mutagenic replication of 8oxoG was observed in crystals of BF bound to template 2 with 8oxoG at the pre-insertion site soaked in 30 mM dATP (60% saturated ammonium sulphate, 0.1 M MES pH 5.8, and 2.5% MPD) or a 30 mM dATP/dTTP mixture (60% saturated ammonium sulphate, 0.1 M Tris pH 8.0, and 2.5% MPD) to observe incorporation or both incorporation and extension, respectively. Crystals were flash frozen in liquid nitrogen for storage and data collection (98 K on a RAXIS IV or RAXIS II detector; or APS beamline 22ID). Data were processed using HKL2000 (ref. 25). All crystals belong to space group $P2_12_12_1$ and contain one molecule per asymmetric unit. Phases were calculated using molecular replacement

(Protein Data Bank entry 1L3S as the probe) and models refined using CNS[26]. CNS topology and parameter files for 8oxoG refinement were generated with PRODRG[27]. Structures were superimposed using the Cα atoms of the palm subdomain (residues 646–655, 823–838, 863–869).

Received 28 May; accepted 2 August 2004; doi:10.1038/nature02908.
Published online 22 August 2004.

1. Lindahl, T. Instability and decay of the primary structure of DNA. *Nature* **362,** 709–715 (1993).
2. Finkel, T. & Holbrook, N. J. Oxidants, oxidative stress and the biology of ageing. *Nature* **408,** 239–247 (2000).
3. Shibutani, S., Takeshita, M. & Grollman, A. P. Insertion of specific bases during DNA synthesis past the oxidation-damaged base 8-oxodG. *Nature* **349,** 431–434 (1991).
4. Greenblatt, M. S., Bennett, W. P., Hollstein, M. & Harris, C. C. Mutations in the p53 tumor suppressor gene: clues to cancer etiology and molecular pathogenesis. *Cancer Res.* **54,** 4855–4878 (1994).
5. Hainaut, P. *et al.* IARC Database of p53 gene mutations in human tumors and cell lines: updated compilation, revised formats and new visualisation tools. *Nucleic Acids Res.* **26,** 205–213 (1998).
6. Lowe, L. G. & Guengerich, F. P. Steady-state and pre-steady-state kinetic analysis of dNTP insertion opposite 8-oxo-7,8-dihydroguanine by *Escherichia coli* polymerases I exo- and II exo. *Biochemistry* **35,** 9840–9849 (1996).
7. Furge, L. L. & Guengerich, F. P. Analysis of nucleotide insertion and extension at 8-oxo-7,8-dihydroguanine by replicative T7 polymerase exo- and human immunodeficiency virus-1 reverse transcriptase using steady-state and pre-steady-state kinetics. *Biochemistry* **36,** 6475–6487 (1997).
8. Freisinger, E., Grollman, A. P., Miller, H. & Kisker, C. Lesion (in)tolerance reveals insights into DNA replication fidelity. *EMBO J.* **23,** 1494–1505 (2004).
9. Johnson, S. J., Taylor, J. S. & Beese, L. S. Processive DNA synthesis observed in a polymerase crystal suggests a mechanism for the prevention of frameshift mutations. *Proc. Natl Acad. Sci. USA* **100,** 3895–3900 (2003).
10. Johnson, S. J. & Beese, L. S. Structures of mismatch replication errors observed in a DNA polymerase. *Cell* **116,** 803–816 (2004).
11. Kiefer, J. R., Mao, C., Braman, J. C. & Beese, L. S. Visualizing DNA replication in a catalytically active *Bacillus* DNA polymerase crystal. *Nature* **391,** 304–307 (1998).
12. Goodman, M. F. Hydrogen bonding revisited: geometric selection as a principal determinant of DNA replication fidelity. *Proc. Natl Acad. Sci. USA* **94,** 10493–10495 (1997).
13. Kool, E. T. Active site tightness and substrate fit in DNA replication. *Annu. Rev. Biochem.* **71,** 191–219 (2002).
14. Miller, H. & Grollman, A. P. Kinetics of DNA polymerase I (Klenow fragment exo-) activity on damaged DNA templates: effect of proximal and distal template damage on DNA synthesis. *Biochemistry* **36,** 15336–15342 (1997).
15. Krahn, J. M., Beard, W. A., Miller, H., Grollman, A. P. & Wilson, S. H. Structure of DNA polymerase beta with the mutagenic DNA lesion 8-oxodeoxyguanine reveals structural insights into its coding potential. *Structure (Camb.)* **11,** 121–127 (2003).
16. Echols, H. & Goodman, M. F. Fidelity mechanisms in DNA replication. *Annu. Rev. Biochem.* **60,** 477–511 (1991).
17. Goodman, M. F., Creighton, S., Bloom, L. B. & Petruska, J. Biochemical basis of DNA replication fidelity. *Crit. Rev. Biochem. Mol. Biol.* **28,** 83–126 (1993).
18. Kunkel, T. A. & Bebenek, K. DNA replication fidelity. *Annu. Rev. Biochem.* **69,** 497–529 (2000).
19. Nair, D. T., Johnson, R. E., Prakash, S., Prakash, L. & Aggarwal, A. K. Replication by human DNA polymerase-ι occurs by Hoogsteen base-pairing. *Nature* **430,** 377–380 (2004).
20. Ling, H., Boudsocq, F., Plosky, B. S., Woodgate, R. & Yang, W. Replication of a cis-syn thymine dimer at atomic resolution. *Nature* **424,** 1083–1087 (2003).
21. Culp, S. J., Cho, B. P., Kadlubar, F. F. & Evans, F. E. Structural and conformational analyses of 8-hydroxy-2′-deoxyguanosine. *Chem. Res. Toxicol.* **2,** 416–422 (1989).
22. Kouchakdjian, M. *et al.* NMR structural studies of the ionizing radiation adduct 7-hydro-8-oxodeoxyguanosine (8-oxo-7H-dG) opposite deoxyadenosine in a DNA duplex. 8-Oxo-7H-dG(syn).dA(anti) alignment at lesion site. *Biochemistry* **30,** 1403–1412 (1991).
23. Kiefer, J. R. *et al.* Crystal structure of a thermostable *Bacillus* DNA polymerase I large fragment at 2.1 Å resolution. *Structure* **5,** 95–108 (1997).
24. Boosalis, M. S., Petruska, J. & Goodman, M. F. DNA polymerase insertion fidelity. Gel assay for site-specific kinetics. *J. Biol. Chem.* **262,** 14689–14696 (1987).
25. Otwinowski, Z. & Minor, W. *Methods in Enzymology, Macromolecular Crystallography (Part A): Processing of X-ray Diffraction Data Collected in Oscillation Mode* (Academic Press, New York, 1997).
26. Brünger, A. T. *et al.* Crystallography & NMR system: A new software suite for marcomolecular structure determination. *Acta Crystallogr. D* **54,** 905–921 (1998).
27. van Aalten, D. M. *et al.* PRODRG, a program for generating molecular topologies and unique molecular descriptors from coordinates of small molecules. *J. Comput. Aided Mol. Des.* **10,** 255–262 (1996).

Supplementary Information accompanies the paper on **www.nature.com/nature**.

Acknowledgements We thank H. W. Hellinga for critical reading of the manuscript. Research was carried out in part at the SER-CAT 22-ID beamline at the Advanced Photon Source (Argonne National Laboratory), which is supported by the US Department of Energy, Office of Energy Research. We also thank J. J. Warren for assistance with data collection. The work was supported by grants to L.S.B. from the National Cancer Institute and the Duke Comprehensive Cancer Center, and to T.C. from the Deutsche Forschungsgemeinschaft, the Volkswagen Stiftung and the Fonds of the German Chemical Industry. M.O. is supported by a fellowship from the Boehringer Ingelheim Foundation.

Competing interests statement The authors declare that they have no competing financial interests.

Correspondence and requests for materials should be addressed to L.S.B. (lsb@biochem.duke.edu). Coordinates have been deposited in the Protein Data Bank under accession codes 1U45, 1U47, 1U48, 1U49 and 1U4B.

Structure of the ESCRT-II endosomal trafficking complex

Aitor Hierro[1], Ji Sun[2], Alexander S. Rusnak[2], Jaewon Kim[1], Gali Prag[1], Scott D. Emr[2] & James H. Hurley[1]

[1]*Laboratory of Molecular Biology, National Institute of Diabetes and Digestive and Kidney Diseases, National Institutes of Health, US Department of Health and Human Services, Bethesda, Maryland 20892-0580, USA*
[2]*Department of Cellular and Molecular Medicine and Department of Chemistry and Biochemistry and Howard Hughes Medical Institute, University of California at San Diego, 9500 Gilman Drive, La Jolla, California 92093-0668, USA*

The multivesicular-body (MVB) pathway delivers transmembrane proteins and lipids to the lumen of the endosome. The multivesicular-body sorting pathway has crucial roles in growth-factor-receptor downregulation[1], developmental signalling[2–4], regulation of the immune response[5] and the budding of certain enveloped viruses such as human immunodeficiency virus[6]. Ubiquitination is a signal for sorting into the MVB pathway[7,8], which also requires the functions of three protein complexes, termed ESCRT-I, -II and -III (endosomal sorting complex required for transport)[7,9,10]. Here we report the crystal structure of the core of the yeast ESCRT-II complex, which contains one molecule of the Vps protein Vps22, the carboxy-terminal domain of Vps36 and two molecules of Vps25, and has the shape of a capital letter 'Y'. The amino-terminal coiled coil of Vps22 and the flexible linker leading to the ubiquitin-binding NZF domain of Vps36 both protrude from the tip of one branch of the 'Y'. Vps22 and Vps36 form nearly equivalent interactions with the two Vps25 molecules at the centre of the 'Y'. The structure suggests how ubiquitinated cargo could be passed between ESCRT components of the MVB pathway through the sequential transfer of ubiquitinated cargo from one complex to the next.

The MVB pathway delivers transmembrane proteins and lipids into small vesicles that invaginate into the lumen of the endosome. MVBs then fuse with the vacuole/lysosome and release the vesicles into the lumen where they are degraded by the hydrolases contained in the vacuole/lysosome[1]. Proteins that remain in the limiting membrane of the MVB are either delivered to the lysosomal/vacuolar limiting membrane or they are recycled to the Golgi complex or the plasma membrane. Therefore, the MVB sorting pathway plays a critical role in the trafficking of numerous cargo proteins within the endosomal membrane system.

Sorting of proteins into the MVB pathway is a complex, multi-step process. It requires coordinated functions of many protein complexes that are conserved from yeast to humans. Screens in *Saccharomyces cerevisiae* have identified numerous genes required for the sorting and trafficking of proteins into the MVB. Mutations in these genes result in defects in the sorting of transmembrane proteins, such as the G-protein-coupled receptor, Ste2p, from the plasma membrane to the vacuolar lumen by means of the MVB pathway. Thus far, more than 20 genes referred to as class E VPS (vesicular protein sorting) genes have been identified[11,12].

During MVB sorting, Hrs–Vps27 is first recruited to the early endosome by virtue of its FYVE domain interaction with PI(3)P (refs 13–15) and its UIM (ubiquitin interacting motif) interaction with ubiquitinated cargo. It then recruits the ESCRT-I complex (composed of Vps23, 28, 37) to the membrane[16]. ESCRT-I recruits the downstream ESCRT-II and ESCRT-III complexes[9]. After the ESCRTs have been recruited to the endosome membrane, the AAA-type ATPase Vps4 binds ESCRT-III and following MVB vesicle formation catalyses the dissociation of the ESCRT protein complexes in an ATP-dependent manner for further rounds of protein sorting[17]. The MVB sorting process is topologically equivalent to the